

# Optimization Design of Fiber-Reinforced Composite Fan Blade with Hollow Structure

Hu Dianyin<sup>2,3,4</sup>, Wu Chao<sup>1</sup>, Liu Xi<sup>1,2,4</sup>, Li Xin<sup>1</sup>, Wang Rongqiao<sup>1,2,4</sup>

<sup>1</sup> School of Energy and Power Engineering, Beihang University, Beijing, China; <sup>2</sup> Beijing Key Laboratory of Aero-Engine Structure and Strength, Beijing, China; <sup>3</sup> Research Institute of Aero-engine, Beihang University, Beijing, China; <sup>4</sup> United Research Center of Mid-Small Aero-Engine, Beijing, China

**Abstract:** Fiber-reinforced composite fan blades, especially hollow fan blades, are gradually applied to civil aero engines, due to their light weight and good vibration damping performance. In this paper, the research on the optimization design method of lay-up angle and hollow structure of fiber-reinforced composite is carried out. Firstly, a modified Tsai-Wu failure criterion considering interlaminar performance was established and validated based on laminate tests. Secondly, the grey relational analysis method is combined with entropy-based weight assignment method to achieve the optimal lay-up angles. This method can visually present the influence degree layer angle of pavement on the quality, strength, vibration, stiffness, and other performance indicators of fan blade. The number of tests required is small and has strong engineering applicability. Then, the parametric modeling method of the hollow structure is developed, and genetic algorithm is combined to achieve optimal design of the hollow structure size. Finally, the two-step optimization iteration of lay-up angles and hollow structure determines the lightweight and high-performance fiber-reinforced composite fan blades. The weight of the hollow fan blade is reduced by 37.0% compared with the initial structure while satisfying the mechanical properties of the blade, which proves the feasibility of the design method and provides technical support for the design of the actual fan blade.

**Keywords:** Fiber-reinforced composite; Hollow structure optimization; Genetic algorithm

## 1 Introduction

Resin-based fiber-reinforced composite fan blades are gradually used in civil turbofan aero-engines due to their light weight and good vibration damping performance [1-3]. To meet the increasing requirements of low fuel consumption and high thrust-to-weight ratio, the future advanced aero-engines are developing in the direction of higher by-pass-ratio and more stable structural mechanical properties. At this time, resin-based composite hollow fan blade with lighter mass and better vibration damping properties are further proposed [4,5]. Meanwhile, preliminary studies have been conducted by Rolls-Royce and other companies to verify the feasibility of resin-based composite hollow fan blades. Therefore, the optimization design of resin matrix composite hollow fan blades is important to improve the engine thrust-to-weight ratio and overall performance.

The optimization design of resin-based composite hollow fan blade requires comprehensive consideration of multiple factors such as mass, strength, vibration, and stiffness, which is a typical multi-objective optimization problem. Peng *et al* [6] transformed the mass, strength, and stiffness objectives into optimization constraints in the multi-objective optimization of lay-up angle and applied a multi-island genetic algorithm to achieve the optimization design. An *et al* [7] transformed the multi-objective lay-up optimization into a single objective by

applying the same weight on each objective and introduced a genetic algorithm to realize the optimization. However, in these optimization approaches, the weights of each performance indicators such as mass, strength, vibration, and stiffness, were determined subjectively, lacking an objective basis. At this time, Jiang *et al* [8] established a lay-up optimization method based on grey relational analysis to achieve the lay-up optimization of composite control arm, in which objective weights of performance indicators were determined through principal component analysis. On this basis, this paper applies the entropy-based weight assignment method [9] to predict the information entropy of each indicator to determine the assigned weights and realize the optimization design of the layup considering the importance.

On the other hand, since the blade shape is pre-determined according to the aerodynamic analysis, the design of hollow structure can further achieve weight reduction and performance optimization. By using the orthogonal test method, Yang *et al* [10] optimize the NACA straight wing type blades to achieve weight reduction. Xiong [11] designed a foam sandwich structure for composite fan blades with significant results in both strength and weight reduction.

Therefore, in this paper, the optimization design of lay-up angle and hollow structure is carried out for resin matrix composite fan blades. Firstly, the grey relational analysis and entropy-based weight assignment method are combined to determine the optimal lay-up angle. Then, the parametric modeling method of hollow structure is developed and combined with the genetic algorithm to realize the optimization design of hollow structure. We also compare and discuss the optimization results with and without using the entropy and grey rational degrees. Finally, the structure of the lightweight and high-performance resin matrix composite hollow fan blade is determined, further providing technical support for the design and application of advanced civil fan engines.

## 2 Optimization framework for composite fan blades

The optimization framework of the composite fan blade is shown in Figure 1. Firstly, the initial configuration of the fan blade is determined based on the aerodynamic blade design. Then, the hollow structure is designed and parametrically modeled. Finally, the optimal lay-up angle was determined by iterating the two iterations to determine the optimal configuration of the resin matrix composite hollow fan blade.

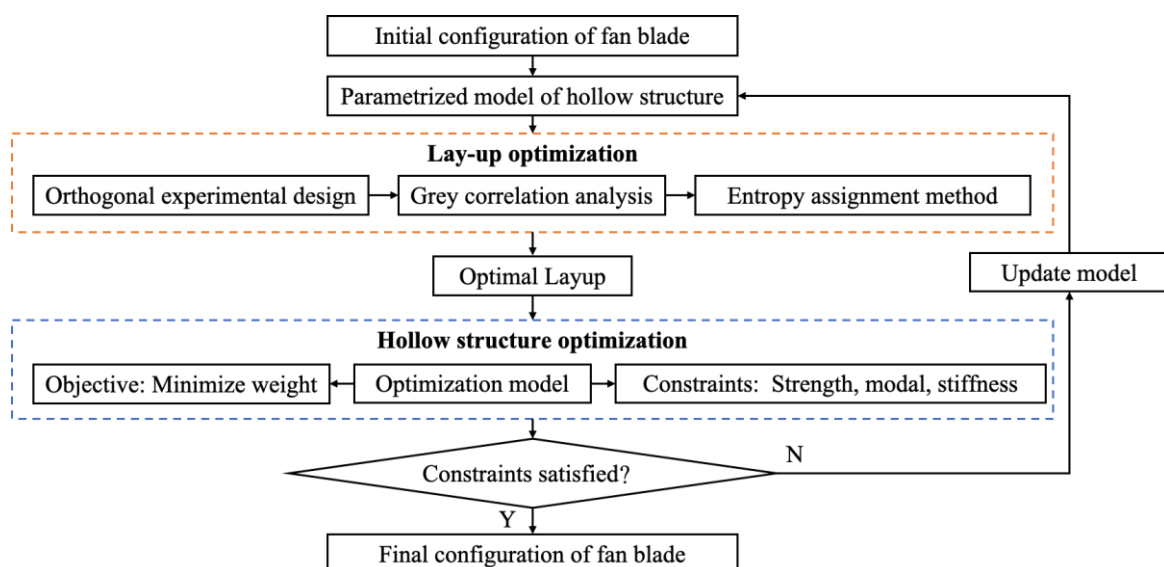


Figure 1 Optimized design framework for composite hollow fan blades

### 3 Initial configuration design of composite hollow fan blade

#### 3.1 Initial configuration design considering process characteristics

The outer shape of the fan blade is shown in Figure 2, in which the height of the blade left side is 542.75 mm, the width of the blade root is 397.76 mm, and the maximum thickness of the blade tip is 13.16 mm. Due to the thin thickness of the fan blade, Polymethacrylimide (PMI) foam sandwich structure [11] was selected as the hollow structure of the fan blade.



Figure 2 Model of fan blade

The three-dimensional (3D) modeling of the hollow structure of the fan blade was carried out with the following steps:

(1) Configuration design of hollow inner cavity section. The cross-section of the hollow inner cavity is obtained by the inward offset of the cross-section of the outer shape. The upper and lower sides of the blade are offset by the same distance (about 3 mm) to ensure the same thickness of covering at the upper and lower surfaces, to avoid the destruction of either side due to the small thickness.

(2) Determination of the location of the hollow inner cavity. Since the blade is mainly subject to centrifugal load, the root part suffers the largest force, while the tip part the smallest. Therefore, the hollow inner cavity is designed to locate at the place near blade tip.

(3) Modelling of the hollow inner cavity. As shown in Figure 3(a), the hollow inner cavity is modeled by combining the contour curves at five cross sections, including the tip section and four body sections.

(4) Modelling of PMI foam sandwich hollow fan blade. The solid blade and the hollow inner cavity are Boolean subtracted to obtain geometry of the hollow fan blade. The hollow inner cavity is the PMI foam core structure model, which is combined with the hollow fan blade to obtain the geometry model of hollow fan blade, as shown in Figure 3(b).

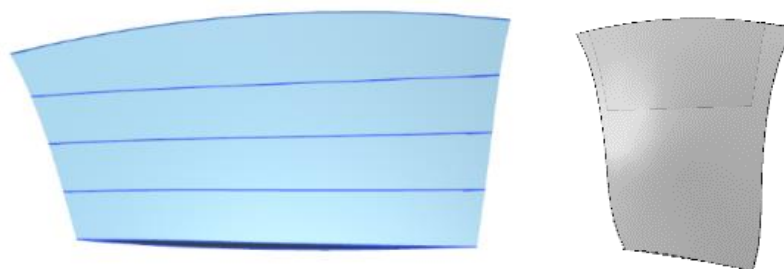


Figure 3 Geometric model of hollow fan blade

### 3.2 Initial design of the lay-up structure

There are generally four lay-up directions for composite structures, namely  $0^\circ$ ,  $\pm 45^\circ$  and  $90^\circ$ . The thickness of the hollow part is about 3mm, while the average thickness of the solid part is about 10mm. Since the thickness of a single layer of the resin-based composite is 0.187mm, the layer numbers of the envelope are set to 16. Based on the symmetrical lay-up principal, and the initial lay-up angle is set to  $[-45,0,0,45,0,0,0,90,0]_s$ . As for the solid part, the layer numbers are set to 48, and the initial lay-up angle is set to  $[-45,0,0,45,0,0,90,0]_{3s}$ . This lay-up form can ensure that the upper and lower surfaces of the blade are paved in the same way, ensuring lay-up continuity of the envelope and the solid parts, thus reducing processing defects. As for the blade root with more than 48 layers, repeat from surface to center in  $[-45,0,0,45,0,0,0,90,0]_s$  pavement pattern, to ensure the continuity of prepreg laying during processing.

### 3.3 Mechanical analysis model

The hollow and solid parts of blade are modeled and meshed by SC8R hexahedral mesh. The hollow fan blade and PMI foam core are glued together. Considering that the foam core is subjected to smaller force and its own strength is much smaller than the gluing, no debonding failure will occur before the foam core fails. Thus, the hollow fan blade and PMI foam core are bound and constrained together during finite element analysis.

The material is T800/X850, with the material properties listed in Table 1.

Table 1 material properties of T800/X850 [12]

| Parameters                        | Symbols | Units | Values |
|-----------------------------------|---------|-------|--------|
| Longitudinal tensile modulus      | $E_1$   | GPa   | 185.0  |
| Transverse tensile modulus        | $E_2$   | GPa   | 9.03   |
| In-plane shear modulus            | $G$     | GPa   | 4.27   |
| Poisson ratio                     | $\nu$   | -     | 0.340  |
| Longitudinal tensile strength     | $X_T$   | MPa   | 2700   |
| Longitudinal compression strength | $X_C$   | MPa   | 1650   |
| Transverse tensile strength       | $Y_T$   | MPa   | 88     |
| Transverse compression strength   | $Y_C$   | MPa   | 225    |
| In-plane shear strength           | $S$     | MPa   | 100    |

The design rotating speed of the fan blade is 3525.64 rpm. The maximum aerodynamic load obtained by the fluid-structure coupling analysis is 5.63 MPa, being much smaller than the centrifugal load. Therefore, the aerodynamic load is simplified to a static load applied to the surface of the hollow fan blade [13]. Meanwhile, a fixed constraint is applied to the blade root.

Before meshing, the hollow fan blade is partitioned into several regions:

- a) Firstly, the solid and hollow parts are partitioned by plane M4;
- b) Then, the regular part in the middle of the blade is partitioned from the conformationally heterogeneous region on both sides by the midpoints, as shown in Figure 4(a);
- c) After the partition is completed, each region chooses different strategies for meshing: in the middle region of the blade (marked green), structured hexahedral mesh is used with high mesh quality and accurate calculation; in both sides of the blade (marked yellow), hexahedral mesh is used to ensure the integrity of the grid structure.

The meshing results are shown in Figure 4 (b), in which the brown color represents the main direction of the lay-up stacking.



Figure 4 Meshing results after partition

The results of the finite element analysis of the initial hollow fan blade are shown in Figure 5. It can be seen from the equivalent stress distribution cloud that the stress at the root of the hollow fan blade is 279.3 MPa. It can be seen that the stress at the hollow fan blade root is the largest, being 279.3MPa. In the bottom of the hollow cavity which is the junction of solid blade and PMI foam core, the stress of the fan blade is significantly increased due to the stress concentration. In Figure 6, we can see that the hollow fan blade root is the dangerous area, with the maximum Tsai-Wu strength factor being 0.503, and the safety factor being  $2.0 > 1.5$ . Although there is stress concentration at the bottom of the hollow inner cavity, Tsai-Wu strength factor compared to the blade root is smaller, and the safety margin is larger. Thus, the bottom of the hollow inner cavity is not considered as a dangerous area for follow-up analysis.

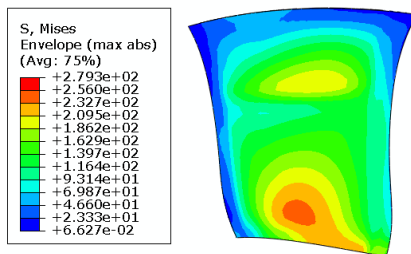


Figure 5 Equivalent stress distribution of hollow fan blade (MPa)

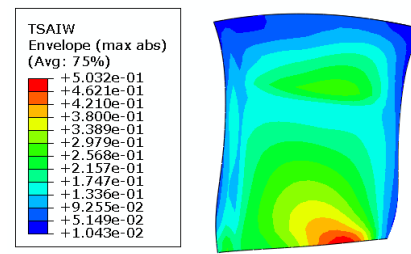


Figure 6 Tsai-Wu strength factor distribution of hollow fan blade (MPa)

PMI foam core is filled in the blade cavity, mainly subject to the stress generated by the blade deformation, and basically does not share the load on the blade. In Figure 7, we can see that the maximum equivalent force is 0.48MPa, the stress is small, in line with the strength requirements.

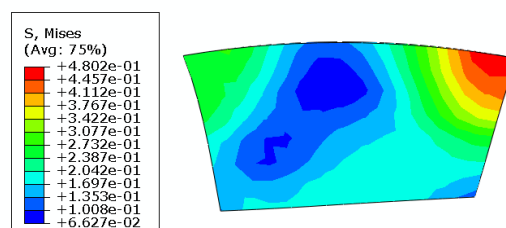


Figure 7 Equivalent stress distribution of PMI foam core (MPa)

In the fan blade design process, the clearance between the tip of the blade and the magazine needs to be strictly controlled; too much clearance will reduce the aerodynamic efficiency, while too little clearance will lead to touch-and-grind failure. On the other hand, the deformation of the fan blade will change its design shape, which in turn will affect the aerodynamic efficiency. Therefore, the stiffness performance of the fan blade needs to be calculated and analyzed, and measures are taken to reduce the deformation of the fan blade.

After the finite element analysis, the deformation distribution of the hollow fan blade is shown in Figure 8. From the total deformation distribution, it can be seen that the deformation of the hollow fan blade's blade tip trailing edge is the largest, being 3.652mm. The maximum deformation and blade body height ratio is less than 1%, to meet the stiffness performance design requirements.

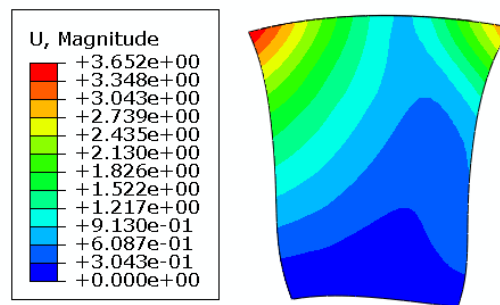


Figure 8 Deformation of hollow fan blade (mm)

## 4 Optimization of lay-up angle

### 4.1 Lay-up angle

The number of layers in the hollow and solid part are different, but the pattern of layers is the same. Thus, the lay-up parameters are eight lay-up angles, with the initial values and the ranges listed in Table 2.

Table 2 Design initial values and range of values for lay-up parameters

| Lay-up angles | Unit | Initial values | Ranges      |
|---------------|------|----------------|-------------|
| $\theta_1$    | °    | -45            | -45;0;45;90 |
| $\theta_2$    | °    | 0              | -45;0;45;90 |
| $\theta_3$    | °    | 0              | -45;0;45;90 |
| $\theta_4$    | °    | 45             | -45;0;45;90 |
| $\theta_5$    | °    | 0              | -45;0;45;90 |
| $\theta_6$    | °    | 0              | -45;0;45;90 |
| $\theta_7$    | °    | 90             | -45;0;45;90 |
| $\theta_8$    | °    | 0              | -45;0;45;90 |

### 4.2 Orthogonal experimental design

Since the lay-up angles are discrete values, the orthogonal experimental design method is introduced to determine the optimal lay-up angles, when the hollow structural size is selected as a certain value. Eight lay-up angles in Table 2 were used as the design factors, while each factor contained four levels, marked as 1=-45°, 2=0°, 3=45°, 4=90°. SPSS software was used to design the orthogonal experiment with 8 factors and 4 levels,

with the orthogonal experiment table  $L_{32}(4^8)$  listed in Table 3.

Table 3 Orthogonal experimental table of lay-up angle

| Scheme | 1 | 2 | 3 | 4 | 5 | 6 | 7 | 8 |
|--------|---|---|---|---|---|---|---|---|
| 1      | 1 | 1 | 1 | 1 | 1 | 1 | 1 | 1 |
| 2      | 1 | 1 | 2 | 4 | 3 | 4 | 2 | 4 |
| 3      | 1 | 2 | 3 | 3 | 2 | 1 | 4 | 4 |
| 4      | 1 | 2 | 4 | 2 | 4 | 4 | 3 | 1 |
| 5      | 1 | 3 | 3 | 1 | 4 | 3 | 4 | 3 |
| 6      | 1 | 3 | 4 | 4 | 2 | 2 | 3 | 2 |
| 7      | 1 | 4 | 1 | 3 | 3 | 3 | 1 | 2 |
| 8      | 1 | 4 | 2 | 2 | 1 | 2 | 2 | 3 |
| 9      | 2 | 1 | 3 | 4 | 1 | 3 | 3 | 3 |
| 10     | 2 | 1 | 4 | 1 | 3 | 2 | 4 | 2 |
| 11     | 2 | 2 | 1 | 2 | 2 | 3 | 2 | 2 |
| 12     | 2 | 2 | 2 | 3 | 4 | 2 | 1 | 3 |
| 13     | 2 | 3 | 1 | 4 | 4 | 1 | 2 | 1 |
| 14     | 2 | 3 | 2 | 1 | 2 | 4 | 1 | 4 |
| 15     | 2 | 4 | 3 | 2 | 3 | 1 | 3 | 4 |
| 16     | 2 | 4 | 4 | 3 | 1 | 4 | 4 | 1 |
| 17     | 3 | 1 | 3 | 3 | 2 | 2 | 2 | 1 |
| 18     | 3 | 1 | 4 | 2 | 4 | 3 | 1 | 4 |
| 19     | 3 | 2 | 1 | 1 | 1 | 2 | 3 | 4 |
| 20     | 3 | 2 | 2 | 4 | 3 | 3 | 4 | 1 |
| 21     | 3 | 3 | 1 | 3 | 3 | 4 | 3 | 3 |
| 22     | 3 | 3 | 2 | 2 | 1 | 1 | 4 | 2 |
| 23     | 3 | 4 | 3 | 1 | 4 | 4 | 2 | 2 |
| 24     | 3 | 4 | 4 | 4 | 2 | 1 | 1 | 3 |
| 25     | 4 | 1 | 1 | 2 | 2 | 4 | 4 | 3 |
| 26     | 4 | 1 | 2 | 3 | 4 | 1 | 3 | 2 |
| 27     | 4 | 2 | 3 | 4 | 1 | 4 | 1 | 2 |
| 28     | 4 | 2 | 4 | 1 | 3 | 1 | 2 | 3 |
| 29     | 4 | 3 | 3 | 2 | 3 | 2 | 1 | 1 |
| 30     | 4 | 3 | 4 | 3 | 1 | 3 | 2 | 4 |
| 31     | 4 | 4 | 1 | 4 | 4 | 2 | 4 | 4 |
| 32     | 4 | 4 | 2 | 1 | 2 | 3 | 3 | 1 |

The three performance indicators of Tsai-Wu strength factor  $TW$ , first-order natural frequency  $F_1$ , and

deformation value  $U$  were calculated for different lay-up angles in Table 3, with the results shown in Figure 9. As can be seen, solutions No. 18, 23, and 31 are the lay-up solutions with the best performances of strength, vibration, and stiffness, respectively. However, none of these solutions can satisfy these three types of performance indicator values at the same time. To balance each indicator, grey relational analysis is introduced to transform multiple performance indicators into grey relational degrees in advance.

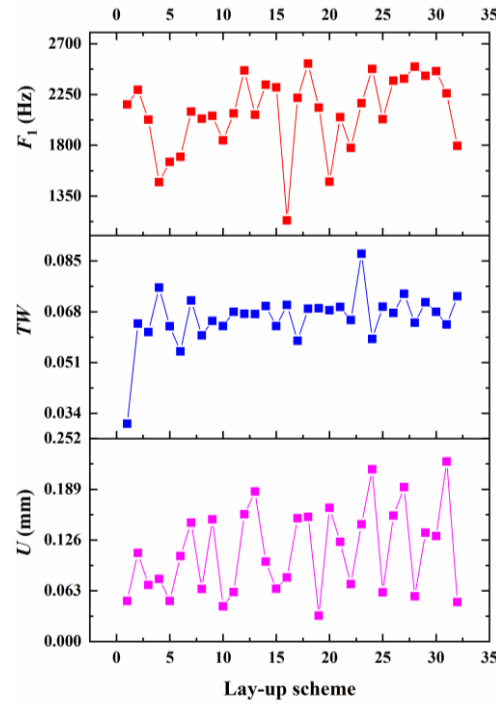


Figure 9 Simulation results of performance index

#### 4.3 Grey relational analysis method

Since the performance indicators in Figure 9 have different magnitudes and the optimization objectives of each indicator are different, the effect of magnitudes is eliminated by normalization. The smaller the Tsai-Wu strength factor  $TW$  and deformation  $U$ , the better the performance, thus the cost-type normalization function is utilized as Eq. (1). The larger the first-order normal frequency  $F_1$ , the better the performance, thus the benefit-type normalization function is applied as Eq. (2).

$$x_i^*(k) = \frac{\max_k x_i(k) - x_i(k)}{\max_k x_i(k) - \min_k x_i(k)} \quad (1)$$

$$x_i^*(k) = \frac{x_i(k) - \min_k x_i(k)}{\max_k x_i(k) - \min_k x_i(k)} \quad (2)$$

in which,  $x_i(k)$  and  $x_i^*(k)$  denote the simulated and normalized values of the  $k$ -th indicator in  $i$ -th scheme, respectively;  $\max_k x_i(k)$  and  $\min_k x_i(k)$  denote the maximum and minimum values of the  $k$ -th indicator, respectively.

After normalization, the larger the normalized indicator value the better the performance, with the minimum value of 0 indicating the worst performance and the maximum value of 1 indicating the best performance. Further, the grey relational coefficient between the normalized index sequence and the optimal solution sequence (taking

the value of 1) is calculated with the follow expression

$$\gamma_{ik} = \gamma(x_0^*(k), x_i^*(k)) = \frac{\Delta_{\min} + \delta\Delta_{\max}}{\Delta_{0i}(k) + \delta\Delta_{\max}}$$

$$\Delta_{\min} = \min_i \min_k \Delta_{0i}(k)$$

$$\Delta_{\max} = \max_i \max_k \Delta_{0i}(k)$$

$$\Delta_{0i}(k) = |x_0^*(k) - x_i^*(k)|$$
(3)

in which,  $\Delta_{0i}(k)$  is the deviation series;  $\Delta_{\min}$  and  $\Delta_{\max}$  denotes the minimum and maximum values of the deviation series, respectively;  $\delta$  denotes the discriminant coefficient, which is taken as 0.5 in this work.

The grey relational coefficients are weighted and summed to obtain the grey relational degree, expressed as

$$\Phi = \sum_{k=1}^n w_k \gamma(x_0^*(k), x_i^*(k))$$
(4)

#### 4.4 Entropy-based weight assignment method

In this work, the entropy value method is used to determine the weight coefficients in the grey relational analysis, to increase the objectivity and credibility of this method.

Firstly, evaluation indicator is formalized and calculated as <sup>[14]</sup>

$$A = (\alpha_{ik})_{n \times m} = \left( \frac{\gamma_{ik}}{\sum_{i=1}^n \gamma_{ik}} \right)_{n \times m}$$
(5)

in which,  $n$  and  $m$  denote the total number of schemes and indicators, respectively. Based on this, the information entropy value of  $k$ -th indicator is calculated and expressed as

$$e_k = -\frac{1}{\ln m} \sum_{i=1}^n \alpha_{ik} \ln \alpha_{ik}$$
(6)

Then the objective weight value calculated can be expressed as

$$w_k = \frac{1 - e_k}{\sum_{i=1}^m (1 - e_k)}$$
(7)

Using the proposed method, the objective weight vector of these three types of indicators is calculated as  $\mathbf{w} = [0.333092, 0.335281, 0.331628]^T$ . The grey relational degrees for 32 schemes were calculated by substituting  $\mathbf{w}$  into Eq. (4), as shown in Figure 10.

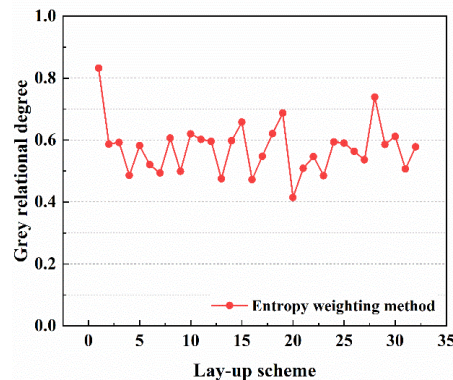


Figure 10 Results of grey relational analysis for lay-up angle

It can be seen from Figure 10 that the grey relational degrees of schemes 1, 19, and 28 are 0.8322, 0.6873, and 0.7389, respectively, which are relatively larger than other schemes. Then, the grey relational degrees of three experimental factors at four levels were calculated and averaged to obtain the average values, as shown in Table 4 and Figure 11, from which, the optimal lay-up angle can be determined as listed in Table 5.

Table 4 The average grey relational values at different levels of the four experimental factors

| Lay-up | Factors | 1      | 2      | 3      | 4      |
|--------|---------|--------|--------|--------|--------|
|        |         | (-45°) | (0)    | (45°)  | (90°)  |
| 1      |         | 0.5875 | 0.5651 | 0.5890 | 0.5506 |
| 2      |         | 0.6076 | 0.5817 | 0.5535 | 0.5493 |
| 3      |         | 0.5613 | 0.5870 | 0.5608 | 0.5831 |
| 4      |         | 0.5482 | 0.5870 | 0.6403 | 0.5167 |
| 5      |         | 0.5394 | 0.5780 | 0.5758 | 0.5990 |
| 6      |         | 0.5329 | 0.5838 | 0.5504 | 0.6251 |
| 7      |         | 0.6071 | 0.5818 | 0.5626 | 0.5407 |
| 8      |         | 0.5490 | 0.6077 | 0.5894 | 0.5460 |

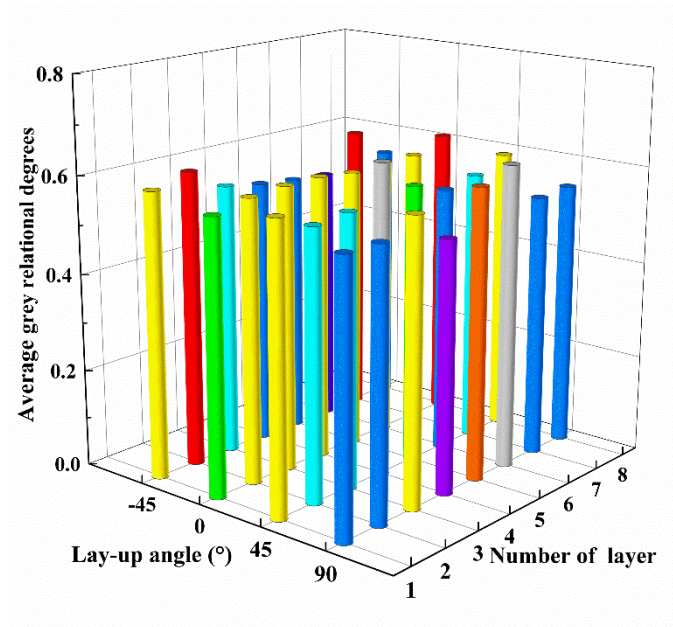


Figure 11 Average grey relational degree

Table 5 Optimal lay-up angle

| Lay-up sequence  | 1  | 2   | 3 | 4  | 5  | 6  | 7   | 8 |
|------------------|----|-----|---|----|----|----|-----|---|
| Lay-up angle (°) | 45 | -45 | 0 | 45 | 90 | 90 | -45 | 0 |

When the entropy and grey relational degrees are not used, the optimization results can be obtained directly by Figure 5. At this time, we need to assign weights to the 3 indicators. Assuming that the assigned weights are 1:1:1, the optimal solution is Scheme 27 in Table 3, as shown in Table 6. However, when the assigned weights change, the optimal solution changes. In this case, the allocation percentage is subjectively determined and has

no basis.

Table 6 Optimal lay-up angle without using the entropy and grey rational degrees

| Lay-up sequence  | 1  | 2 | 3  | 4  | 5   | 6  | 7   | 8 |
|------------------|----|---|----|----|-----|----|-----|---|
| Lay-up angle (°) | 90 | 0 | 45 | 90 | -45 | 90 | -45 | 0 |

## 5 Optimization of hollow configuration

### 5.1 Parametric modeling of hollow structures

The hollow inner cavity consists of fitted contour curves of five cross sections, where the plane above the blade tip section is the fixed datum plane, numbered as  $M_0$ . The remaining four reference planes are numbered as  $M_1$ - $M_4$ , with the positioning parameters for basic plane being  $H_1$ - $H_4$ , as shown in Figure 12.

The contour curves of the hollow inner cavity on the  $M_0$ - $M_4$  reference planes are numbered as  $N_0$ - $N_4$ , while the offset distance parameters of these five contour curves are  $A_0$ - $A_4$ . The parametric design strategy is used to simplify the nine independent parameters ( $H_1$ - $H_4$ ,  $A_0$ - $A_4$ ) into 3 independent parameters to improve the efficiency of parametric modeling. The results of the parametric design are shown in Table 7.

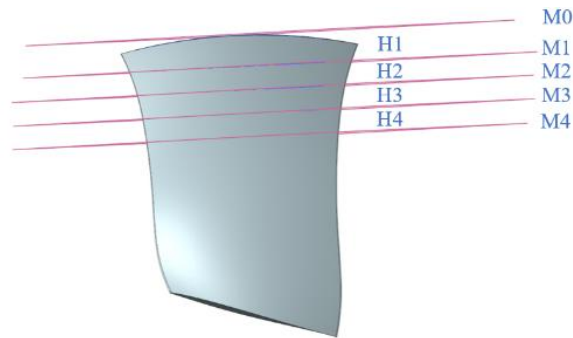


Figure 12 Basic plane of hollow inner cavity and its position parameters

Table 7 Design results of hollow inner cavity parameters

| Parameters | Symbols | Units |
|------------|---------|-------|
| $H_1$      | $H$     | mm    |
| $H_2$      | $E$     | mm    |
| $H_3$      | $E$     | mm    |
| $H_4$      | $E$     | mm    |
| $A_0$      | $0.76G$ | mm    |
| $A_1$      | $0.82G$ | mm    |
| $A_2$      | $0.85G$ | mm    |
| $A_3$      | $0.9G$  | mm    |
| $A_4$      | $G$     | mm    |
| $H$        | 40-90   | mm    |
| $E$        | 50-140  | mm    |
| $G$        | 3.7-6.5 | mm    |

Finally, three key parameters in the hollow fan blade geometry model were determined, which are parameters  $H$  and  $E$  that determine the position of the hollow inner cavity blade section, and parameter  $G$  that determines the offset distance of the hollow inner cavity blade section. The initial values and the ranges for these three key parameters are shown in Table 8.

Table 8 Design initial values and range of values of hollow structure size parameters

| Parameters | Initial values (mm) | Ranges (mm) |
|------------|---------------------|-------------|
| $H$        | 60                  | 40-90       |
| $E$        | 60                  | 50-140      |
| $G$        | 4.0                 | 3.7-6.5     |

### 5.2 Optimization constraints

To ensure that the structural mechanical properties of the hollow fan blade meet the design requirements, the strength, stiffness, and modal properties are used as constraints in the optimization design process.

According to the safety design requirements of composite structure, the strength margin of hollow fan blade should larger than 1.5. Meanwhile, considering that the fan blade is exposed to hot and humid environment, the influence of the environment should also be considered, with the environmental factor being taken as 1.5. In addition, since the ratio of ultimate speed to operating speed is usually 1.22, a safety margin for the ultimate speed is required in the design of strength performance. In summary, the safety factor of the hollow fan blade should be larger than 2.745, which means that the Tsai-Wu strength factor is less than 0.364.

To ensure that the blade tip clearance meets the design requirements to avoid the impact of blade deformation on aerodynamic performance, the deformation value of the blade needs to be controlled within a certain range. Therefore, 1% of the blade body length, i.e. 5.43mm, is used as a constraint for the blade stiffness performance.

The vibration analysis is carried out to obtain the Campbell diagram, as shown in Figure 13. As can be seen, if the first-order natural frequency is too small, it will intersect with the isochronous speed line and cause resonance of the fan blade. Therefore, the first-order natural frequency of the fan blade should be greater than 71 Hz.

In summary, the constraints are obtained as shown in Table 9.

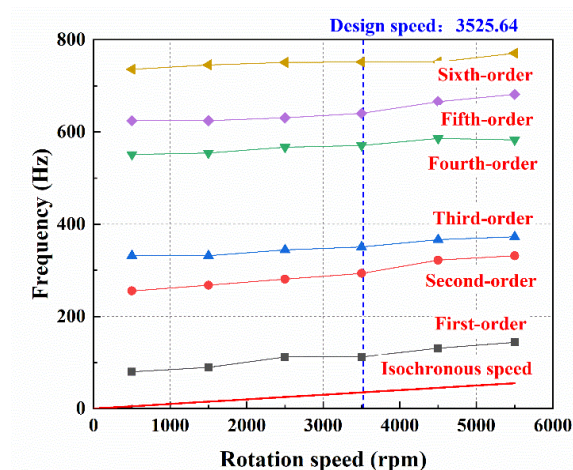


Figure 13 Hollow fan blade Campbell diagram

Table 9 Constraints of parameters

| Parameters                    | Symbols | Constraints |
|-------------------------------|---------|-------------|
| Tsai-Wu strength factor       | $TW$    | $< 0.364$   |
| First-order natural frequency | $F_1$   | $> 71$ Hz   |
| Deformation                   | $U$     | $< 5.43$ mm |

### 5.3 Optimization goals

The optimization objective is to minimize the weight. Considering that the density of composite materials is generally  $1.5\text{-}1.8\text{g/cm}^3$ , and the density of PMI foam is  $0.075\text{g/cm}^3$  which can be neglected, the total volume  $V$  of hollow fan blade is taken as the mass function.

### 5.4 Optimization model

The expression of the optimization problem is

$$\begin{aligned}
 &\text{find } \mathbf{x} = (x_1, x_2, x_3)^T \\
 &\min W(\mathbf{x}) \\
 &\text{st.} \begin{cases} 40 \leq x_1 \leq 100 \\ 50 \leq x_2 \leq 140 \\ 3.7 \leq x_3 \leq 6.5 \\ F_1(\mathbf{x}) > 71 \\ TW(\mathbf{x}) < 0.364 \\ U(\mathbf{x}) < 5.34 \end{cases} \quad (8)
 \end{aligned}$$

in which,  $x_1 \sim x_3$  are the dimensional parameters of the hollow structure;  $W(\mathbf{x})$  is the mass function, i.e., the volume of blade.

### 5.5 Optimization results

The genetic algorithm was used to optimize the equation with the range of optimization parameters shown in Table 8. In genetic algorithm, the number of populations was set to 20, the orphan size was set to 5, the total number of evolutionary generations was set to 20, and the crossover probability was set to 0.9. After 2000 cycles, the optimization results were obtained with the optimization history plotted in Figure 14.

The optimized size of the hollow structure is  $E=138.8$  mm,  $G=3.8$  mm,  $H=98$  mm, in which case the total volume of the hollow fan blade is minimum  $1744471$   $\text{mm}^3$ . After optimization, the total volume is reduced by 37.0% compared with the initial state, which has a good weight reduction effect. At this time, the blade first-order natural frequency is 61 Hz, the maximum Tsai-Wu strength factor is 0.352, and the maximum deformation is 2.60 mm, which satisfies the design requirements.

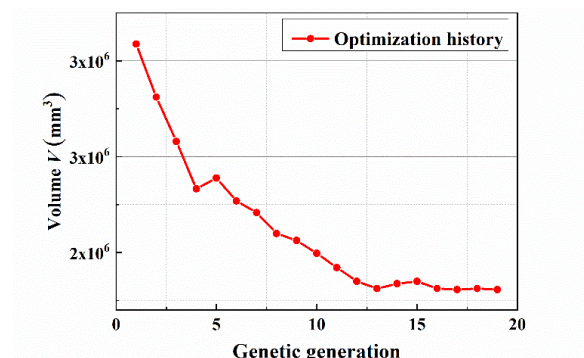


Figure 14 Optimization history

The stress and deformation distributions after optimization are shown in Figure 15 and Figure 16, respectively. It can be found that the maximum Tsai-Wu strength factor decreases after optimization and the position changes, shifting from the hollow fan blade root to the blade body.

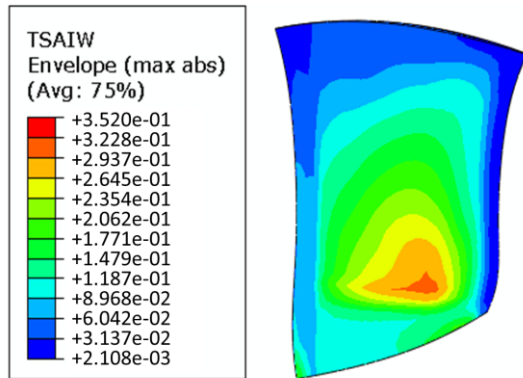


Figure 15 Tsai-Wu strength factor distribution of hollow fan blade after optimization (MPa)

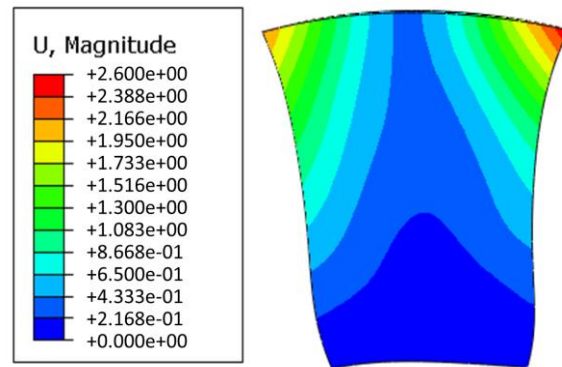


Figure 16 Deformation of hollow fan blade after optimization (mm)

Also, the optimal lay-up angle distribution Table6 is obtained by the direct optimization method, and the hollow structure is optimized, and the optimized stress and deformation distributions are shown in Figure 17 and Figure 18, respectively. It can be found that the maximum Tsai-Wu and deformation are larger than the results in Figure 15 and Figure 16, which verifies the rationality of the optimization method using the entropy and grey rational degrees.

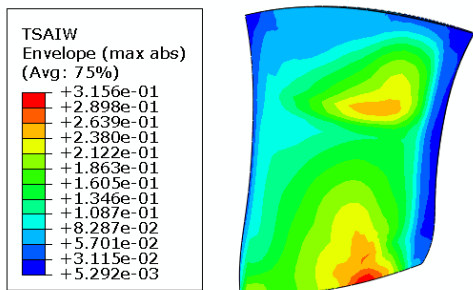


Figure 17 Tsai-Wu strength factor distribution of hollow fan blade after optimization (MPa)

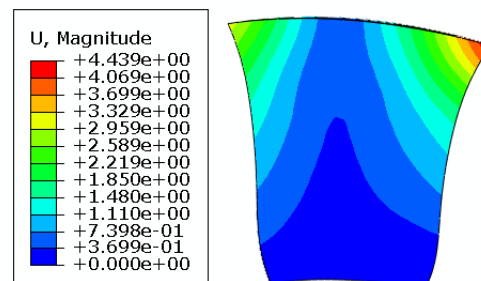


Figure 18 Deformation of hollow fan blade after optimization (mm)

## 6 Conclusion

An optimal design method for composite hollow fan blades was established. The orthogonal test-assignment grey relational analysis method is used to realize the optimization of composite lay-up angle, and the hollow structure size is optimized based on genetic algorithm. The detailed conclusions are listed as follows:

(1) The optimization design process for composite hollow fan blades is established. Aiming at discrete ply angle variables and continuous hollow size variables, a sequential iteration method was applied to achieve an optimal design.

(2) The gray relational analysis method with entropy-based weight is used to optimize the lamination angle of composite materials, which intuitively shows the impact of each layer's lamination angle on quality, strength,

vibration, stiffness, and other performance indicators.

(3) An efficient parametric modeling method for composite hollow fan blades was established, and the size of the hollow structure was optimized based on a genetic algorithm. Results show that, on the premise of meeting the mechanical properties of the blade structure, the weight of the hollow fan blade is reduced by 37.0% compared with the initial hollow structure, verifying the feasibility of the design method and providing an technical support for actual fan blade structural design.

Meanwhile, the limitation and prospects of this paper can be summarized as follows.

(1) Modal tests and static strength tests of composite fan blades are carried out to verify the accuracy of the structural mechanical analysis methods.

(2) This paper only analyzes the strength, stiffness, and modal properties of the fan blade, for the structural design of the fan blade, research in the areas of impact damage and fatigue life is still required.

#### Acknowledgements

This work was supported by National Natural Science Foundation of China (NSFC) [grant numbers 52022007, 51875020, and 52105138]; the Major National Science and Technology Projects in China [grant numbers 2017-IV-0004-0041, J2019-IV-0016-0084, and J2019-IV-0009-0077].

#### References:

- [1] Amoo L M. On the design and structural analysis of jet engine fan blade structures[J]. *Progress in Aerospace Sciences*, 2013, 60: 1-11.
- [2] Sreejith M, Rajeev R S. Fiber reinforced composites for aerospace and sports applications[M]//Fiber Reinforced Composites. Woodhead Publishing, 2021: 821-859.
- [3] Sheikhi M R, Aygun H, Altuntas O. Aeroengines: Principles, Components, and Eco-friendly Trends[M]//Materials, Structures and Manufacturing for Aircraft. Cham: Springer International Publishing, 2022: 127-151.
- [4] Parveez B, Kittur M I, Badruddin I A, et al. Scientific advancements in composite materials for aircraft applications: a review[J]. *Polymers*, 2022, 14(22): 5007.
- [5] Pope G G. Aeronautical technology-recent advances and future prospects[J]. *The Aeronautical Journal*, 1995, 99(983): 81-89.
- [6] Hu D, Peng M, Wang R, et al. Optimization design of resin-based composite fan blade[J]. *Journal of Aerospace Power*, 2012, 27(7): 1630-1637.
- [7] An H, Chen S, Huang H. Multi-objective optimal design of hybrid composite laminates for minimum cost and maximum fundamental frequency and frequency gaps[J]. *Composite Structures*, 2019, 209: 268-276.
- [8] Jiang R, Ci S, Liu D, et al. Ply optimization of carbon fiber reinforced plastic control arm based on grey relational analysis[J]. *Acta Materiae Compositae Sinica*, 2022, 39(1): 9.
- [9] Zhou M, Liu X B, Yang J B, et al. Evidential reasoning approach with multiple kinds of attributes and entropy-based weight assignment[J]. *Knowledge-Based Systems*, 2019, 163: 358-375.
- [10] Yang J, Wang R. Structural optimization of hollow fan blade based on orthogonal experimental design [J]. *Journal of Aerospace Power*, 2011,26(2):376-384.
- [11] Xiong J, Du Y, Mousanezhad D, et al. Sandwich Structures with Prismatic and Foam Cores: A Review[J]. *Advanced Engineering Materials*, 2018, 21(1).

- 
- [12] Wang C, Chen Y, An Q, et al. Drilling temperature and hole quality in drilling of CFRP/aluminum stacks using diamond coated drill [J]. *International Journal of Precision Engineering and Manufacturing*, 2015(16), 1689-1697.
- [13] Qi S, Wang Y, Shi P, et al. A novel numerical-verified approach on reinforcing open-hole composites with tailored variable angle tow patches [C]. *1st International Conference on Theoretical, Analytical and Computational Methods for Composite Materials and Composite Structures*. Wuhan, China, 2018.
- [14] Wu B, Lu M, Lei, et al. Research on optimal scheme of tunnel construction based on orthogonal test and combined weighting grey correlation method[J]. *Journal of Safety Science and Technology*, 2019, 15(8): 124-130.